Picosecond strain pulses probed by the photocurrent in semiconductor devices with quantum wells

D. Moss, A. V. Akimov,[*] R. P. Campion, M. Henini, C. T. Foxon, L. Eaves, and A. J. Kent
School of Physics and Astronomy, University of Nottingham, University Park, Nottingham NG7 2RD, United Kingdom

B. A. Glavin
Institute of Semiconductor Physics, National Academy of Sciences, Kiev 03028, Ukraine
(Received 10 February 2011; revised manuscript received 6 April 2011; published 6 June 2011)

Ultrafast acoustic wave packets are detected by probing the photocurrent in semiconductor devices containing quantum wells. The strain pulses were generated by thermalization of a femtosecond laser pulse in a thin metal film deposited on the surface of the GaAs substrate opposite to the semiconductor device. The probing was realized by measuring the photocurrent excited by a femtosecond optical pulse with photon energy close to the excitonic resonance of the quantum well. Two types of devices are used: a reverse biased (AlGa)As *p-i-n* tunneling diode containing a GaAs quantum well in its intrinsic region and a planar device containing an (InGa)As quantum well. The change in photocurrent arises from the strain-induced shift of the quantum well excitonic resonance due to deformation potential electron-phonon coupling. The method has a picosecond temporal resolution, shows a high sensitivity to subterahertz acoustic wave packets and has potential for ultrafast control of electrical conductance in semiconductor devices.

DOI: 10.1103/PhysRevB.83.245303 PACS number(s): 72.80.Ey, 72.50.+b, 85.30.Mn

I. INTRODUCTION

Since the work by Thomsen *et al.*,[1] experiments with picosecond strain pulses have shown the way to extend traditional low frequency and megahertz acoustics to the gigahertz and terahertz (10^9–10^{12} Hz) frequency ranges. During the past decade, a research field called *picosecond acoustics* has become firmly established and offers the prospect of forthcoming applications for GHz and THz elastic waves in communications and imaging. Various techniques for the generation and detection of coherent acoustic wave packets, strain pulses and solitons using ultrafast lasers have been developed.[2] A large number of recent experiments have used picosecond acoustic wave packets to probe semiconductor nanostructures, including superlattices,[3–6] phonon microcavities,[7,8] quantum wells,[9–13] *p-n* and Schottky diodes,[14,15] and heterojunctions.[16] The results demonstrate the feasibility of exploiting semiconductor nanostructures as components in THz acoustic devices[17,18] and integrated ultrafast optical and electronic circuits.

The traditional techniques for studying acoustic wave packets with pico- and femtosecond temporal resolution are based on the detection of the probe optical pulses reflected (transmitted) from (through) the object under investigaton.[19–21] These well-developed methods, which are similar to traditional pump-probe techniques used in ultrafast optics, provide valuable information about the properties of high-frequency acoustic waves and their interaction with electronic excitations. However, these techniques possess quite low sensitivity and limited spatial resolution. For instance, the relative acoustic modulation amplitude of the optical pulse reflected from a metal film on the surface of a material has a value of a similar order to the strain amplitude η_0 in the acoustic wave packet.[21] The amplitude of coherent Brillouin signals,[19,20] governed by the elasto-optical constants, have similar values. Exploiting the resonance properties of optical transitions (e.g., excitons in quantum wells[11]) does not increase the sensitivity to the elastic waves significantly.

Increasing the sensitivity and improving the spatial resolution for the detection of THz sound are challenging tasks, which may have a large impact on the realization of various new ideas and concepts in hypersonics.[22] One way to achieve these goals could be to electrically probe coherent acoustic wave packets instead of measuring the intensity of the reflected or transmitted optical signals. In the case of electrical detection of acoustic waves in nano devices, the spatial resolution is defined by the size of the device which in the case of semiconductor nanostructures may be as small as few nanometers. High sensitivity could be realized by exploiting the strain sensitive electrical transport properties of semiconductor devices.[15,23] The temporal resolution of the electrically detected THz acoustic wave packet could be performed by using microwave[24] or pump-probe photocurrent techniques[25] as recently tested successfully in experiments with strain pulses.

In this paper we demonstrate how coherent acoustic wave packets can be detected with subpicosecond time resolution by probing photocurrent in various semiconductor transport devices containing a quantum well (QW). The method is shown conceptually in Fig. 1 and is based on the strong sensitivity of the optical resonance energy E_0 of a semiconductor QW to the strain η (i.e., the piezospectroscopic effect[26,27]). The vertical line in Fig. 1 indicates the optical transition which falls into the low-energy side of the electron-hole resonance shown by the shaded area. Optical excitation of carriers causes a photocurrent I_p, which is proportional to the number of photoexcited carriers n_c and depends on the proximity of the photon energy of the optical excitation, $\hbar\omega$, to the values of E_0. In practice I_p depends on the detuning $\Delta = E_0 - \hbar\omega$: The value of I_p is maximum when $\Delta = 0$ and I_p decreases when $|\Delta|$ increases. The effect of the strain is to change E_0. It is well known that for the deformation potential mechanism, the energy shift $\delta E_0 = \Xi\eta$, where Ξ is the deformation potential. In the example shown in Fig. 1, $E_0 > \hbar\omega$ and $\Xi<0$. Consequently, the compressive strain

 ©2011 American Physical Society

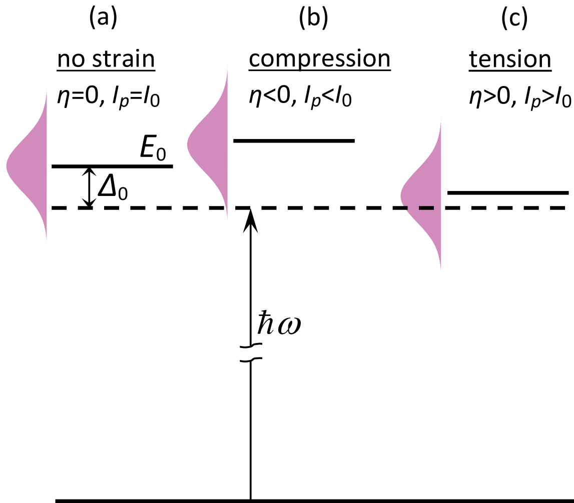

FIG. 1. (Color online) Diagramatic representation of the sensitivity of the photocurrent I_p in a semiconductor QW to strain η (piezospectroscopic effect). I_0 and Δ_0 are the stationary photocurrent and detuning respectively, present when $\eta = 0$.

($\eta < 0$) induces an increase in E_0 and, therefore, Δ increases [Fig. 1(b)]. The increase in Δ results in a decrease in n_c and respectively, I_p. When $\eta > 0$ (tension) the opposite scenario happens: Δ decreases while n_c and I_p increase [Fig. 1(c)].

In nonstationary experiments with picosecond longitudinal (LA) strain pulses $\eta(t,x)$ (x is the direction of the strain pulse propagation), the values of $\Delta(t)$, $n_c(t)$, and $I_p(t)$ are time-dependent functions and, in general, their temporal evolutions require special consideration with respect to the specific

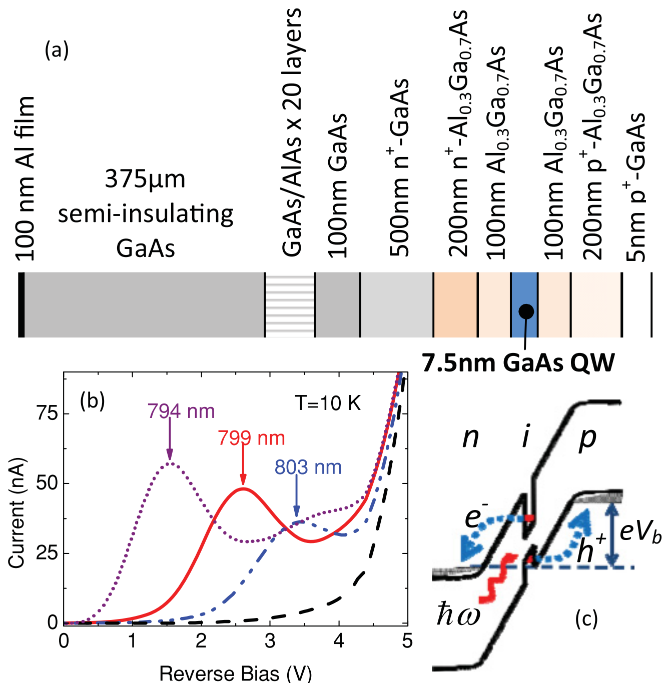

FIG. 2. (Color online) (a) The scheme of layers in the *p-i-n* device including a QW. (b) *IV* characteristics of the device under illumination from a cw laser with various wavelengths and in the dark (dashed line). (c) The band diagram of the *p-i-n* device.

optical resonance and transport properties of the object under study. However, we shall concentrate on a thin semiconductor QW located in a plane perpendicular to the x axis. In this case, the nonstationary piezospectroscopic effect can be described in a simple way when the pulsed optical excitation is almost instantaneous at $t = t_0$ and $\eta(t,x)$ in the QW can be considered independent of x at each moment t. Such an approximation is usually valid in the experiments when strain pulses have a duration ~10 ps and the QW width is $d_{QW} \sim 10$ nm.[12] Then

$$\Delta(t) = \Xi\eta(t,x_0) + \Delta_0, \tag{1}$$

where x_0 is the position of the QW and Δ_0 is the detuning at $\eta = 0$. In the linear approximation, which works when $\Delta(t)$ is much smaller than the spectral width of the optical (i.e., exciton) resonance, the time-integrated photocurrent change can be written as

$$I_p(t_0) - I_0 \propto \Xi\eta(t_0,x_0). \tag{2}$$

Where I_0 is the photocurrent at $\eta = 0$.

Thus by measuring $I_p(t_0)$ as a function of t_0, which is controlled by the delay between the strain and probing optical pulses, it is possible to obtain the temporal evolution of the strain $\eta(t,x_0)$ in the QW embedded in a transport semiconductor device.

In the present work we perform a detailed study of picosecond strain pulses measured by probing the photocurrent in vertical and lateral semiconductor transport devices incorporating QWs. We analyze the measured signals as a function of the bias voltage applied to the devices and wavelength of probe light which excites the photocurrent. Section II describes the two types of semiconductor device and details of the technique used in the experiments. In Sec. III we present the experimental results and accompanying qualitative discussion. This section consists of three subsections, where the results for a vertical tunneling *p-i-n* junction with a QW in the insulator layer (Sec. III A) and planar device containing two QWs with different d_{QW} (Sec. III B) are presented. Section III C gives the quantitative analysis of the strain induced effects of the QW containing devices, and conclusions are given in Sec. IV.

II. SAMPLES AND EXPERIMENTAL TECHNIQUES

A. Tunneling *p-i-n* junction with a quantum well

The composition of the multilayer *p-i-n* tunneling diode used in our experiment is shown in Fig. 2(a). The layers were grown by molecular beam epitaxy (MBE) on a semi-insulating GaAs substrate of a thickness $l = 375$ μm. The active structure included a sequence of layers forming a *p-i-n* junction with a single 7.5-nm-wide QW between two 100-nm-wide undoped $Al_{0.3}Ga_{0.7}As$ barriers. The n and p contacts were, respectively, Si-doped and C-doped (both 10^{18} cm^{-3}) 200-nm-wide layers of $Al_{0.3}Ga_{0.7}As$. The wafer was processed into 200-μm-diameter mesas with ring-shaped contact metallization to allow optical access.

In the dark the device shows current-voltage $I(V_b)$ characteristics typical for a *p-i-n* junction: The current increases rapidly with the increase of forward bias, and the device starts to emit light. The application of large reverse bias results

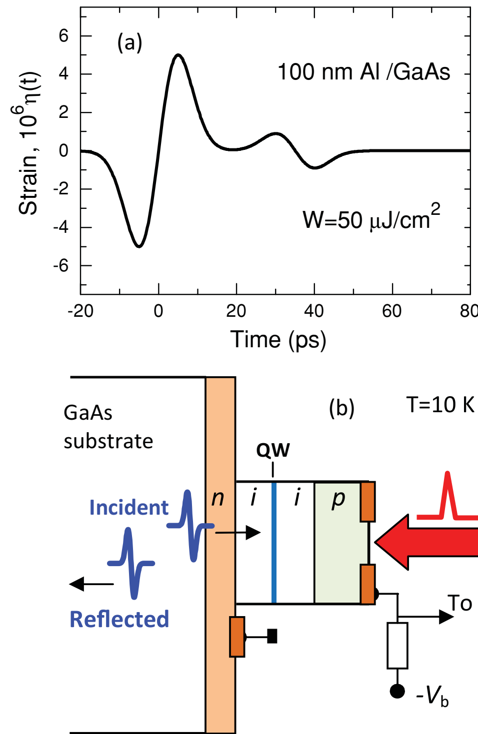

FIG. 3. (Color online) (a) The temporal profile of the strain pulse generated in the Al film and injected into the GaAs substrate. (b) The experimental scheme for strain-pulse detection in the *p-i-n* device.

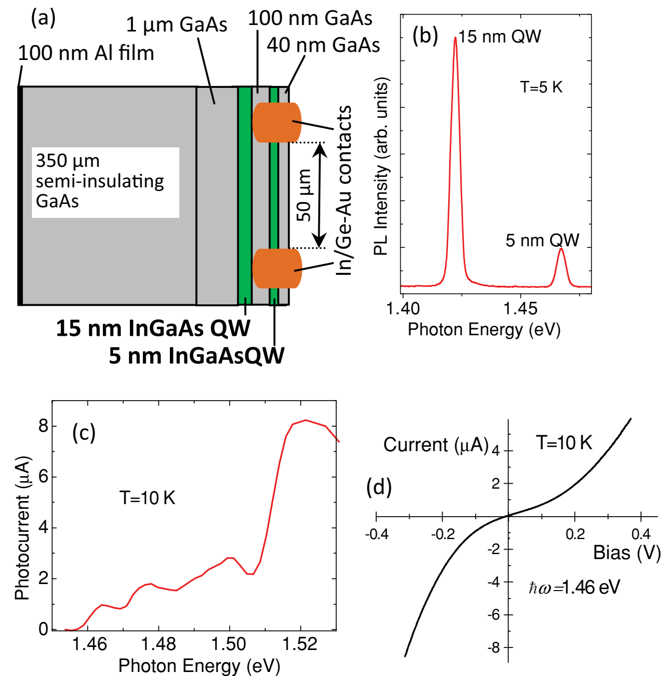

FIG. 4. (Color online) (a) Structural schematic of the lateral device sample which includes two QWs. (b) The photoluminescence spectrum of the sample. (c) The photocurrent spectrum measured for cw excitation. (d) *IV* characteristic of the device when the QW, situated closest to the surface, is optically excited by a cw laser.

in breakdown at around $V_b = 4 \div 9$ V, depending on the particular device. At lower reverse bias, illumination of the device induces a strong photocurrent. The $I(V_b)$ curves for three excitation wavelengths and in the dark, all measured at temperature $T = 10$ K, are shown in Fig. 2(b). Figure 2(c) illustrates the corresponding band diagram of the device under reverse bias. The peaks [marked by vertical arrows in Fig. 2(b)] in the *IV*s under illumination, with a maximum dependent on the excitation wavelength, are well known to be related to the exciton transition in the QW.[28] Indeed a peak should occur when $\hbar\omega = E_0$. The value of E_0 decreases with increasing V_b in accordance with quantum-confined Stark effect for excitons.[29] Thus with decreasing $\hbar\omega$ (i.e., increase of the excitation wavelength) the peak should occur at higher V_b. Such behavior can be tracked in Fig. 2(b) and in the reverse bias regime we find:

$$E_0(\text{eV}) = -9 \times 10^{-3} V_b + 1.58, \quad (3)$$

which fits well to the calculated dependence for the *p-i-n* device with the given parameters.

In the ultrafast experiments, the picosecond strain pulses were generated in a 100-nm-thick Al film deposited on the polished side of the GaAs substrate opposite to the *p-i-n* structure. The film was excited by ~150-fs optical pump pulses from a titanium-sapphire laser with a repetition rate 82 MHz. The laser beam was focused on the surface of the Al film to a spot with a diameter of 50 μm exactly opposite to the optical mesa of the *p-i-n* structure. Due to the thermoelastic effect, a 10-ps duration bipolar strain pulse $\eta(t,x)$ was generated in the film.[30,31] Here x is the coordinate perpendicular to the interface of the substrate with the metal film. The strain pulse is injected from the Al film into the substrate where it propagates with the velocity of longitudinal (LA) sound in GaAs, $s_L = 4.8 \times 10^3$ m/s, and reaches the device at time $\tau_0 = l/s_L = 73$ ns. The excitation density in the pump pulse did not exceed $W_{\text{max}} \sim 60\ \mu\text{J/cm}^2$. This gives the maximum estimated strain amplitude $\eta_0 \sim 5 \times 10^{-6}$,[30] which corresponds to the linear propagation regime for the strain pulse through the GaAs substrate, and at low temperatures ($T < 50$ K) the attenuation in GaAs can be ignored.[32] The calculated temporal profile of the $\eta(t)$ for arbitrary x in GaAs is shown in Fig. 3(a) and includes a bipolar strain pulse form followed by an echo due to reflections in the Al film.

The experiments were performed in a cryostat at $T = 10$ K. The experimental setup for detecting the effect of the strain pulse in the *p-i-n* device is shown in Fig. 3(b). The device was excited by a femtosecond optical probe beam split from the same laser that was used to excite the Al film. The pump beam was passed through a step-motor optical delay line which provided a time delay t_0 between strain and probe pulses. The probe beam was focused to a spot of 20 μm at the center of the optical mesa with an average power density <1 kW/cm^2. The photocurrent induced by the probe pulse was amplified, and the time-integrated signal I_p measured as a function of the time delay t_0. In order to pick out the strain-induced signal $\Delta I_p(t_0) = I_p(t_0) - I_0$ (I_0 is the signal without a strain pulse), the pump pulse was modulated at a frequency 80 kHz and a lock-in amplifier was used to detect $\Delta I_p(t_0)$.

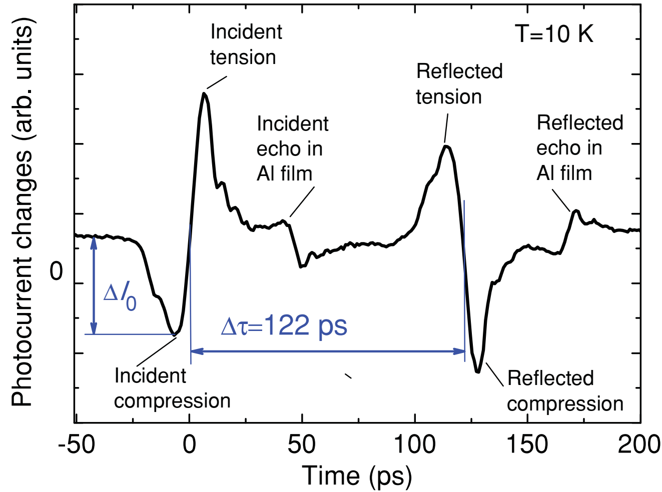

FIG. 5. (Color online) Photocurrent changes as a function of the delay between pump and probe measured in the *p-i-n* device for $\hbar\omega = 1.56$ eV ($\lambda = 795$ nm), $V_b = 3.2$ V, pump density 55 μJ/cm^2, average probe power density 500 W/cm^2. The value $t_0 = 0$ corresponds to probing when the middle of the incident strain pulse passes the QW.

B. Lateral transport device with two quantum wells

A schematic diagram of the planar transport devices containing two QWs is shown in Fig. 4(a). The structure was grown by MBE on 350-μm-thick GaAs substrate. The device includes two $In_{0.08}Ga_{0.92}As$ QWs with widths of 15 and 5 nm. The thicknesses of the GaAs barriers were 100 nm between the QWs and 40 nm and 1 μm from the top surface and substrate, respectively. All layers were nominally undoped. The In/Ge-Au contacts were diffused into the layers and the active size of the transport device between the contacts was 50×50 μm^2.

Figure 4(b) shows the photoluminescence (PL) spectrum of the structure measured at $T = 5$ K. The spectrum, consisting of two lines, gives the exciton energies in QWs, $E_0^{(w)} = 1.423$ eV and $E_0^{(n)} = 1.467$ eV in the wide and narrow QWs, respectively. We measured the low-temperature photocurrent spectrum [Fig. 4(c)] of the device for steady state optical excitation from a Ti-sapphire laser. The significant increase in current is observed at $\hbar\omega > 1.46$ eV when the excitons and carriers are excited in the narrow QW, which is the closest to the surface. The increase in photocurrent for $\hbar\omega > 1.51$ eV is related to the excitations in the GaAs barriers. The structure in the spectrum for 1.46 eV $< \hbar\omega <$ 1.51 eV is due to the optical transitions between the excited states for electrons and holes in the narrow QW. In measurements with the photoexcitation chopped at a frequency of 1 kHz, the photocurrent was also detected when only the wide QW was excited [$E_0^{(w)} < \hbar\omega < E_0^{(n)}$]. The difference between dc and ac measurements is due to the non-ohmic behavior of the device contacts, which is typical for low temperature measurements in undoped devices. In this case, capacitive conductance in ac measurements becomes essential and an ac photocurrent is detected even when dc resistance is high. The nonlinearity of the dc-$I(V)$ curve, shown in Fig. 4(d), is a clear indication of the non-ohmic nature of the contacts.

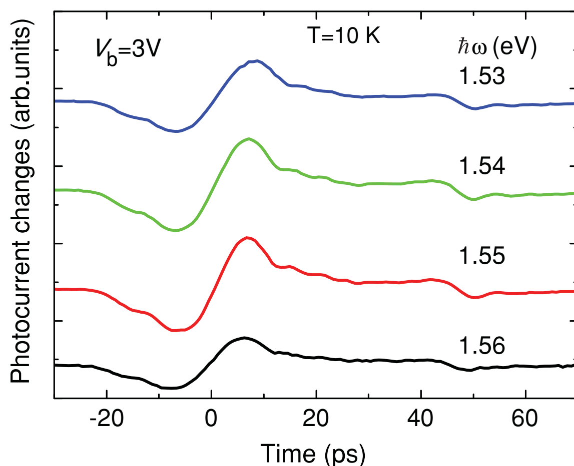

FIG. 6. (Color online) Photocurrent changes $\Delta I_p(t_0)$ which occur when the incident strain pulse passes the *p-i-n* device QW for various probe photon energies $\hbar\omega$, with $W = 60$ μJ/cm^2 and probe power density 100 W/cm^2.

The ultrafast strain pulse experiments were performed in a similar way to that described for the *p-i-n* diode devices. Particular care was taken to control the position of the probe beam on the device mesa. The examples of the photocurrent spectrum and $I(V)$ curve shown in Figs. 4(c) and 4(d) correspond to the case when the photoexcitation is centered between the contacts. For photoexcitation near the contacts, there is a background photocurrent at zero bias which is due to photovoltaic effects in the near-contact regions.

III. EXPERIMENTAL RESULTS AND DISCUSSION

A. *p-i-n* junctions

An example of a temporal trace of the photocurrent changes $\Delta I_p(t_0)$ probed in the *p-i-n* device is shown in Fig. 5 for $\hbar\omega = 1.56$ eV and $V_b = 3.2$ V. The main features of the temporal pump-probe signal are two bipolar pulses that correspond to the incident and reflected strain pulses arriving to the QW from the GaAs substrate and the surface of the sample, respectively. These pulses have opposite phases in agreement with the reflection of elastic waves at the free surface. The delay $\Delta\tau$ between the pulses corresponds to the propagation time for the acoustic wave packet from the QW to the surface and back. The measured value, $\Delta\tau = 122$ ps, is in full agreement with the expected delay of 128 ps, calculated from the layer thicknesses shown in Fig. 2(a). The small difference between the expected and measured values of $\Delta\tau$ is probably due to a small uncertainty in the calibration of layer thickness during the MBE growth process. The signal $\Delta I_p(t_0)$ (Fig. 5) also possesses features from additional strain pulses with lower amplitude which are delayed relative to the main bipolar strain pulses by 47 ps. These pulses are the echoes generated as a result of reflections of the strain pulse at the surfaces of the Al film [see Fig. 3(a)].

The temporal evolution $\Delta I_p(t_0)$ follows the expected evolution of strain $\eta(t,x)$ for $x = x_0$ where the QW is located. This key experimental observation provides unambiguous evidence that the strain pulse is detected with picosecond resolution and it is probed only in the QW embedded in the

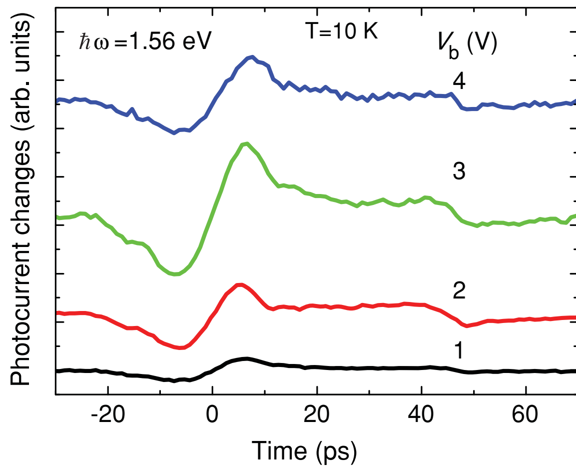

FIG. 7. (Color online) Photocurrent changes $\Delta I_p(t_0)$ when the incident strain pulse is passing the QW of the *p-i-n* device for various reverse bias voltages V_b , with $\hbar\omega = 1.56$ eV, $W = 60$ μJ/cm^2 and probe power density 100 W/cm^2.

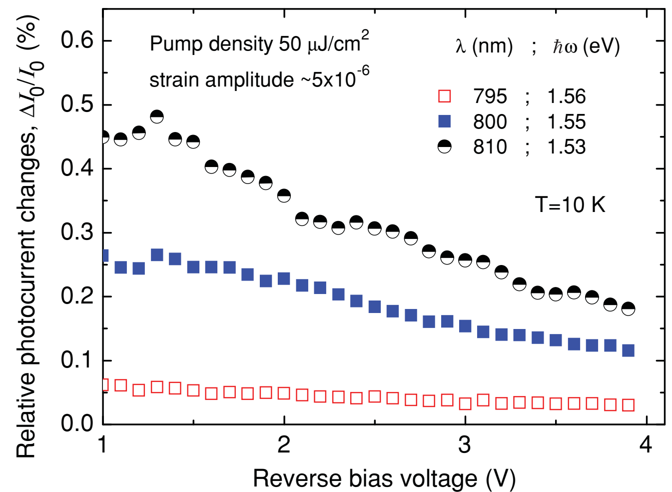

FIG. 9. (Color online) Relative photocurrent changes $\Delta I_0/I_0$ measured in *p-i-n* device as a function of reverse bias voltage and various probe excitation wavelengths λ (photon energies $\hbar\omega$).

device. If other contributions (e.g., the effects on the carrier tunneling rates or strain induced effects in the contacts) to $\Delta I_p(t_0)$ exist, they give slower signals, which are determined by the external circuit of the device. Indeed, in Fig. 5 a constant background is clearly seen, but it is not so big as to mask the fast temporal signal $\Delta I_p(t_0)$ and we shall not consider it further.

In the following, we describe how the signals $\Delta I_p(t_0)$ depend on the photon excitation energy $\hbar\omega$ and V_b, concentrating specifically on the time interval corresponding to the incident strain pulse. The reflected strain pulse is always a mirrored repetition of the incident pulse with corresponding phase changes. First we consider the temporal evolution of $\Delta I_p(t_0)$ and then turn to the analysis of its amplitude. Figure 6 shows the measured signals $\Delta I_p(t_0)$ for $V_b = 3$ V and several different values of $\hbar\omega$. It is seen that signal amplitude varies for different $\hbar\omega$, but the temporal shape of $\Delta I_p(t_0)$ remains exactly the same. The temporal shape was also found to be

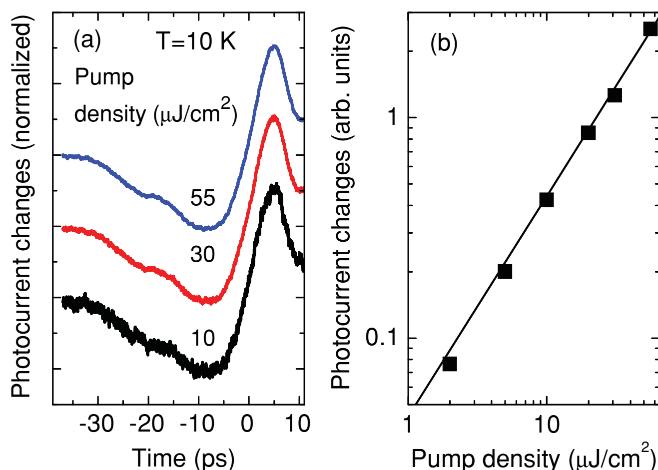

FIG. 8. (Color online) (a) Photocurrent changes $\Delta I_p(t_0)$ when the incident strain pulse is passing the QW of the *p-i-n* device for various pump densities W at the Al film, $V_b = 3$ V , $\hbar\omega = 1.56$ eV. (b) The dependence of the changes of photocurrent amplitude ΔI_0 on pump density W; the solid line is the linear fit.

independent on V_b (Fig. 7). As $\hbar\omega$ and V_b are varied, the characteristics of the diode change dramatically, which can be seen in the *IV* curves shown in Fig. 2(b). We estimate variation in electron tunneling time to range from ~1 ns to ~1 ps due to changes in barrier profiles [Fig. 2(c)] brought about by increasing the negative bias from $V_b = 0$ to $V_b = 6$ V. The independence of the temporal shape with respect to $\hbar\omega$ and V_b supports our conclusion regarding detection of the ultrafast signal $\Delta I_p(t_0)$ in the imbedded QW, while all other parts of the device do not give any fast contribution to $\Delta I_p(t_0)$. This fact is used in the analysis in Sec. III C where only the number of photoexcited carriers in the QW is considered to be sensitive to the dynamical strain.

For the excitation pump densities W used in our experiments, the temporal profile of $\Delta I_p(t_0)$ is independent of W and the amplitude ΔI_0 (for a definition of ΔI_0 see Fig. 5) is proportional to W (see Fig. 8). The result shows that there are no nonlinearities in the mechanism of detection of strain pulses for values of $W < W_{\max}$ used in the present experiments. Neither did we find any nonlinearities in the response of the signal as the probe fluence was increased up to an average power density of 500 W/cm^2 (at the focus on the optical mesa). These results are different from the data obtained in our earlier work[25] where much higher values for W and probe fluence were used.

Studying the temporal profiles for different values of $\hbar\omega$, V_b, and W leads us to conclude that the picosecond time resolution of the detection technique is limited by the time of flight of the acoustic pulse across the QW. For our experiment, this time is around 2 ps, which is a reasonable value for ultrafast acoustic experiments.

Now we turn to the analysis of the amplitude ΔI_0 of the signal $\Delta I_p(t_0)$ and its dependence on $\hbar\omega$ and V_b. For convenience of presentation, and the requirements of further quantitative analysis presented in Sec. III C, we shall consider a ratio $\Delta I_0/I_0$ (I_0 is the photocurrent measured in the absence of the strain pulses). The dependencies of $\Delta I_0/I_0$ on V_b for three values of $\hbar\omega$ are shown in Fig. 9. It is seen that $\Delta I_0/I_0$

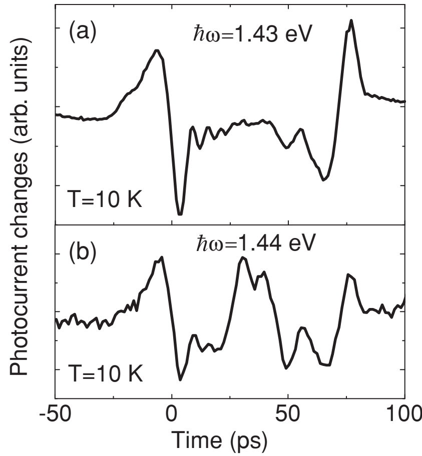

FIG. 10. Photocurrent changes as function of delay time, measured in the lateral device with two QWs: (a) $\hbar\omega = 1.43$ eV ($\lambda = 865$ nm), only wide QW is excited; (b) $\hbar\omega = 1.44$ eV ($\lambda = 860$ nm), both QWs are excited by the probe beam.

decreases with increasing $\hbar\omega$ and V_b. The value $\Delta I_0/I_0$ is proportional to the strain amplitude η_0:

$$\Delta I_0/I_0 = \alpha\eta_0, \tag{4}$$

where α is the sensitivity of the device to strain. The value of α, determined from the results shown in Fig. 9, depends on $\hbar\omega$ and V_b. Note the high sensitivity of the measured signals to strain pulses. Indeed, in our experiments, for maximal strain amplitude $\eta_0 \sim 5 \times 10^{-6}$, $\hbar\omega = 1.53$ eV, and $V_b = 1$ V, the value $\Delta I_0/I_0 \approx 5 \times 10^{-3}$ corresponds to sensitivity $\alpha \sim 10^3$ which is three orders of magnitude higher than that of traditional ultrafast acoustic techniques where the measured changes in the reflectivity from the surface is of similar order to the strain amplitude. The quantitative analysis of the mechanisms which give such high value for α in the *p-i-n* device is given in Sec. III C.

B. Lateral transport device

The lateral photocurrent devices also show the potential for highly sensitive detection of picosecond acoustic wave packets. Figure 10 shows the temporal evolution of $\Delta I_p(t_0)$ measured in the device with two QWs described in Sec. IIB. The most interesting result is the dependence of the temporal shape of $\Delta I_p(t_0)$ on the probe excitation energy $\hbar\omega$. At $\hbar\omega = 1.43$ eV [Fig. 10(a)] the temporal shape is similar to the $\Delta I_p(t_0)$ measured for the *p-i-n* diode structure where only one QW exists [compare Fig. 5 with Fig. 10(a)]. In both cases the main contributions to $\Delta I_p(t_0)$ come from two bipolar pulses which arrive at a given QW from two opposite directions: from the substrate and after reflection from the free GaAs surface. For the lateral device, when $\hbar\omega = 1.43$ eV [Fig. 10(a)] there is no evidence of a contribution to $\Delta I_p(t_0)$ from the narrower QW, which is located closer to the surface than the wide QW. This is consistent with the basic concept of the probing mechanism which relies on the piezospectrscopic effect (Fig. 1). Indeed, for $\hbar\omega = 1.43$ eV the narrow QW is not excited because the photon energy of the excitation is smaller than the energy of the exciton resonance. Thus only the wide QW is excited for $\hbar\omega = 1.43$ eV. When $\hbar\omega = 1.44$ eV, which is closer to the edge for the excitation of photocurrent in the narrow QW [see Fig. 4(c)], additional peaks in $\Delta I_p(t_0)$ appear in the time interval $t = 25$–50 ps. These are due to detection of the forward and reflected strain pulses in the narrow QW which is closer to the surface of the sample.

These results demonstrate the possibility of probing acoustic wave packets in embedded layers by photocurrent techniques and of determining the depth of the layers from a surface. The procedure is based on the simple approach of determining the distance as a product of the sound velocity and time $\Delta\tau$ between the incident and reflected pulses. For instance, at $\hbar\omega = 1.43$ eV, we obtain $\Delta\tau = 72$ ps. This gives the location of the wide QW to be 170 nm from the surface, which is more accurate than the value of 152 nm obtained from MBE calibration performed in several runs before the sample was grown.

The temporal shape of $\Delta I_p(t_0)$ in lateral photocurrent devices did not depend on the bias voltage. However, care was taken in optimizing the bias voltage and positioning of the focused probe beam on the device in order to achieve maximal signal-to-noise ratio. A built-in potential is present in the near contact regions due to their non-ohmic features. The signal was also detected at zero bias if the pump-probe spots were together displaced to one side of the device. However, the non-ohmic characteristics of the contacts do not affect the temporal and spatial vertical resolution for probing the strain pulses. The signal still shows sharp temporal peaks and it is sensitive to $\hbar\omega$.

C. Analysis of the sensitivity to strain

In the devices studied here the time-integrated photocurrent generated by the carriers excited optically in the QW may be written as:[33]

$$I_p = \frac{2en_c\tau_{\rm rad}}{\tau_t + \tau_{\rm rad}}, \tag{5}$$

where n_c is the number of electron-hole pairs photoexcited in the QW due to light absorption, $\tau_{\rm rad}$ is carrier recombination time in the QW, and τ_t is the time characterizing the carrier escape from the QW. In the *p-i-n* diode, which we will consider first, τ_t is the time of carrier tunneling from the QW to the AlGa As *i* regions. For the experimental device, the tunneling time τ_t for the electrons is much less than that for holes and for the bias voltages of interest the values of $\tau_t \ll \tau_{\rm rad} \sim 1$ ns. Therefore, from Eq. (5) it is found that the major fraction of photoexcited carriers contribute to the photocurrent rather than to radiative recombination.

The number of photoexcited electrons and holes is given by

$$n_c = \int P(E)A(E)dE, \tag{6}$$

where $P(E)$ is the spectral density of the optical energy flux and $A(E)$ is the QW absorption efficiency. In ultrafast experiments $P(E)$ can be approximated by a Gaussian,

$$P(E) \sim \exp\left[-\frac{(E-\hbar\omega)^2}{2(\hbar\Delta\omega)^2}\right], \tag{7}$$

with the broadening parameter $\hbar\Delta\omega \approx 8.2$meV measured for our probe optical pulse.

In the analysis of the strain-induced photocurrent, we first assume that the kinetic parameters τ_t and τ_{rad} are insensitive to strain. Then the strain-induced changes of I_p are governed only by the modification of $A(E)$. The spectral shape of $A(E)$ can be modeled by the curves shown in the insets of Fig. 11. The peak, which is present only in the inset of Fig. 11(b), and the high-energy wing correspond to the exciton and free electron-hole transitions, respectively.[28] The strain η modifies $A(E)$ by changing the energy separation E_0 between the quantized electron and hole states in the QW. First we shall consider the modulation of E_0 due to the deformation potential mechanism. Then $A(E) = A_0(E) - \frac{dA_0}{dE}\Xi\eta$, where $A_0(E)$ is the absorption spectrum at $\eta = 0$ and Ξ is the deformation potential which includes strain-induced effects for both electrons and holes (for GaAs $\Xi \approx -10$ eV[34]). Consequently, the strain-induced relative changes in the photocurrent can be written as:

$$\frac{I_p - I_0}{I_0} = -\frac{\Xi\eta \int P(E)\frac{dA_0(E)}{dE}dE}{\int P(E)A_0(E)dE}, \tag{8}$$

where I_0 is the photocurrent without the strain pulse.

In addition to the deformation potential, there are other mechanisms which can cause strain induced changes in $A(E)$. Strain in the QW results in the variation of (i) the dielectric constant and, correspondingly, the electric field in the QW;[35] (ii) the QW width;[36] and (iii) the effective mass.[37] All of these contributions shift the electron and hole levels in the QW and modify the overlap of the confined electron and hole wave functions. However, numerical estimates show that for the structures used in the experiments, these mechanisms provide a total contribution to the photocurrent that is at least an order of magnitude weaker than that due to the deformation potential.

Figure 11 shows the bias dependences of the sensitivity α for the *p-i-n* device, which were calculated using Eq. (8). The theoretical results are presented in the insets for two model dependencies of $A_0(E)$. Figure 11(a) corresponds to the case when exciton effects are ignored and $A_0(E)$ shows only the edge corresponding to interband transitions in the QW. In Fig. 11(b) the exciton peak is included. The values of $\hbar\omega$ are chosen in accordance with the values used in the experiments and the range of variable V_b corresponds to conditions when $\hbar\omega \approx E_0$ which follows from Eq. (3). It is seen that the value of α and its dependence on V_b are very sensitive to $\hbar\omega$. This dependence is especially strong when the exciton peak is well pronounced in $A_0(E)$ [Fig. 11(b)], in which case, α can even change sign. The calculated values of α are up to 10^3 and comparable with values obtained in the experiments.

The peaks in the measured stationary $I(V)$ curves [Fig. 2(b)] show that the exciton contribution exists in $A_0(\omega)$ for the *p-i-n* device. However, it is difficult to estimate its intensity relative to the free electron-hole transitions which result in the high-energy background. There are also uncertainties in the exciton binding energy and spectral width in the presence of the electric field. In the calculated curves [Fig. 11(b)] these values are taken to be 5 and 20 meV respectively. In reality, the exciton spectrum is more complicated than a single line and includes the peaks related to the excited states. From the rough comparison of the calculated curves (Fig. 11) with the experimental data (Fig. 9) we may say that the experimental situation is probably somewhere in between the extreme cases presented in Figs. 11(a) and 11(b).

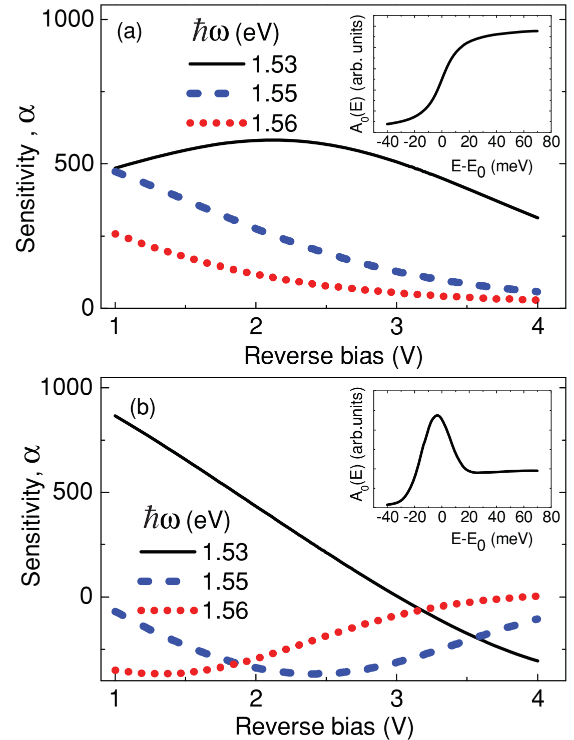

FIG. 11. (Color online) Calculated dependencies of the sensitivity, α, of the *p-i-n* device to strain as a function of reverse bias for three different probe excitation energies with a spectral width of 20 meV and where (a) only interband electron-hole transitions are taken into account; (b) exciton transitions are included in absorption spectrum. Insets show the corresponding spectral profiles, $A_0(E)$, of the optical absorption.

The above analysis based on Eq. (5) assumes that the kinetic parameters τ_t and τ_{rad} are strain independent. This assumption is justified for the *p-i-n* device by the experimental result that shows no dependence of the temporal shape $\Delta I_p(t)$ on V_b (Fig. 7). Indeed, any strain induced changes of τ_t or τ_{rad} would be detected in the time interval that the carriers are present in the QW after the probe pulse. Then $\Delta I_p(t)$ will be the result of the time convolution of the strain pulse $\eta(t)$ and temporal decay of the photoexcited carriers in the QW. The estimated values of $\tau_t \sim 1-100$ ps vary by orders of magnitude in the range of V_b studied. Therefore if τ_t and τ_{rad} did depend on strain, the temporal shape of $\Delta I_p(t)$ would be strongly dependent on V_b, but this is not observed in the *p-i-n* device experiments. The situation is different for the lateral device where the electric field in the regions far from the contacts is not large enough to provide fast separation of photogenerated electrons and holes. The Gaussian intensity profile of the laser spot should be also taken into account in the analysis. That is why the quantitative analysis in lateral devices is more uncertain and additional work is required which will be presented in later publications.

IV. CONCLUSIONS

We have shown that the probing of photocurrent in semiconductor devices with nanolayers can work as a highly

sensitive method for detecting ultrafast acoustic wave packets. The structures can be designed as vertical or lateral transport devices and should possess an optical resonance. The temporal resolution has a value of several picoseconds and is limited by the time of flight for sound through the active nanolayer. The devices used in our experiments have a sensitivity to picosecond strain pulses of up to three orders of magnitude higher than the conventional pump-probe techniques that are widely used in picosecond acoustics. The developed technique shows a potential for probing with nanometer spatial resolution embedded nanostructures that possess an optical resonance. Various nanostructures can be distinguished when the energies of optical resonance have different values. Spatial resolved detection of the acoustic wave packets becomes possible using spatially extended devices and scanning the probe spot.

The main mechanism for the probing technique in the present work is the piezospectroscopic effect, governed by the deformation potential electron-phonon interaction. It is clear that the dynamical piezospectroscopic effect can be even stronger if other mechanisms give additional contributions. One mechanism which should give an effect is the piezoelectric mechanism of electron-phonon interaction, which becomes significant in materials such as GaN-based nanostructures[6,14,24] or GaAs layers grown on high index crystallographic surfaces. The strain-induced modulation of nanostructure dimensions (known as the ripple mechanism) may become significant in structures incorporating quantum dots.[38] Also, structures grown on low-symmetry surfaces may be used for the detection of shear acoustic waves.

The observed effects of strain pulses on the photocurrent are strong enough to use this technique for the ultrafast control of transport properties. The devices used in the present work are not designed as ultrafast electrical devices, but it is clear that using smaller junctions will reduce the capacitance of the device, which opens the prospect of controlling photocurrent on an ultrafast time scale using picosecond acoustic techniques.

ACKNOWLEDGMENTS

We acknowledge the financial support from the Engineering and Physical Sciences Research Council and Royal Society for financial support.

*andrey.akimov@nottingham.ac.uk

[1] C. Thomsen, H. T. Grahn, H. J. Maris, and J. Tauc, Phys. Rev. B **34**, 4129 (1986).

[2] en.wikipedia.org/wiki/Picosecond_ultrasonics

[3] A. Yamamoto, T. Mishina, Y. Masumoto, and M. Nakayama, Phys. Rev. Lett. **73**, 740 (1994).

[4] A. Bartels, T. Dekorsy, H. Kurz, and K. Köhler, Phys. Rev. Lett. **82**, 1044 (1999).

[5] W. Chen, Y. Lu, H. J. Maris, and G. Xiao, Phys. Rev. B **50**, 14506 (1994).

[6] C.-K. Sun, J.-C. Liang, and X.-Y. Yu, Phys. Rev. Lett. **84**, 179 (2000).

[7] M. F. Pascual Winter, G. Rozas, A. Fainstein, B. Jusserand, B. Perrin, A. Huynh, P. O. Vaccaro, and S. Saravanan, Phys. Rev. Lett. **98**, 265501 (2007).

[8] A. Huynh, B. Perrin, N. D. Lanzillotti-Kimura, B. Jusserand, A. Fainstein, and A. Lemaître, Phys. Rev. B **78**, 233302 (2008).

[9] J. J. Baumberg, D. A. Williams, and K. Köhler, Phys. Rev. Lett. **78**, 3358 (1997).

[10] O. Matsuda, T. Tachizaki, T. Fukui, J. J. Baumberg, and O. B. Wright, Phys. Rev. B **71**, 115330 (2005).

[11] A. V. Akimov, A. V. Scherbakov, D. R. Yakovlev, C. T. Foxon, and M. Bayer, Phys. Rev. Lett. **97**, 037401 (2006).

[12] A. V. Scherbakov, P. J. S. van Capel, A. V. Akimov, J. I. Dijkhuis, D. R. Yakovlev, T. Berstermann, and M. Bayer, Phys. Rev. Lett. **99**, 057402 (2007).

[13] T. Berstermann, A. V. Scherbakov, A. V. Akimov, D. R. Yakovlev, N. A. Gippius, B. A. Glavin, I. Sagnes, J. Bloch, and M. Bayer, Phys. Rev. B **80**, 075301 (2009).

[14] K. H. Lin, C.T. Yu, Y. C. Wen, and C. K. Sun, Appl. Phys. Lett. **86**, 093110 (2005).

[15] D. M. Moss, A. V. Akimov, B. A. Glavin, M. Henini, and A. J. Kent, Phys. Rev. Lett. **106**, 066602 (2011).

[16] S. H. Lee, A. L. Cavalieri, D. M. Fritz, M. C. Swan, R. S. Hegde, M. Reason, R. S. Goldman, and D. A. Reis, Phys. Rev. Lett. **95**, 246104 (2005).

[17] A. J. Kent, R. N. Kini, N. M. Stanton, M. Henini, B. A. Glavin, V. A. Kochelap and T. L. Linnik, Phys. Rev. Lett. **96**, 215504 (2006).

[18] R. P. Beardsley, A.V. Akimov, M. Henini, and A. J. Kent, Phys. Rev. Lett. **104**, 085501 (2010).

[19] H. N. Lin, R. J. Stoner, H. J. Maris, and J. Tauc, J. Appl. Phys. **69**, 3816 (1991).

[20] B. Wright, J. Appl. Phys. **71**, 1617 (1992).

[21] E. Péronne and B. Perrin, Ultrasonics **44**, e1203 (2006).

[22] T. Gorishnyy, M. Maldovan, C. Ullal, and E. L. Thomas, Phys. World **18**, 24 (2005).

[23] D. R. Fowler, A. V. Akimov, A. G. Balanov, M. T. Greenaway, M. Henini, T. M. Fromhold, and A. J. Kent, Appl. Phys. Lett. **92**, 232104 (2008).

[24] M. R. Armstrong, E. J. Reed, Ki-Yong Kim, J. H. Glownia, W. M. Howard, E. L. Piner and J. C. Roberts, Nature Physics **5**, 285 (2009).

[25] D. Moss, A. V. Akimov, O. Makarovsky, R. P. Campion, C. T. Foxon, L. Eaves, A. J. Kent, and B. A. Glavin, Phys. Rev. B **80**, 113306 (2009).

[26] E. F. Gross and A. A. Kaplyanskii, Sov. Phys. Solid State **2**, 1518 (1961).

[27] M. Cardona, *Modulation Spectroscopy* (Academic Press, New York, 1969).

[28] S. Schmitt-Rink, D. S. Chemla, and D. A. B. Miller, Adv. Phys. **38**, 89 (1989).

[29] D. A. B. Miller, D. S. Chemla, T. C. Damen, A. C. Gossard, W. Wiegmann, T. H. Wood, and C. A. Burrus, Phys. Rev. B **32**, 1043 (1985).

[30] G. Tas and H. J. Maris, Phys. Rev. B **49**, 15046 (1994).

[31] O. B. Wright, Phys. Rev. B **49**, 9985 (1994).

[32]B.W. Chen, H. J. Maris, Z. R. Wasilewski, and S. Tamura, Philos. Mag. B **70**, 687 (1994).
[33]B. F. Levine, J. Appl. Phys. **74**, R1 (1993).
[34]F. H. Pollak and M. Cardona, Phys. Rev. **172**, 816 (1968).
[35]B. A. Glavin, V. A. Kochelap, T. L. Linnik, and K. W. Kim, Phys. Rev. B **71**, 081305(R) (2005).
[36]F. T. Vasko and V. V. Mitin, Phys. Rev. B **52**, 1500 (1995).
[37]V. I. Pipa, V. V. Mitin, and M. Stroscio, Appl. Phys. Lett. **74**, 1585 (1999).
[38]P. A. Knipp and T. L. Reinecke, Phys. Rev. B **52**, 5923 (1995).